Int J Adv Manuf Technol (2008) 38:904–914
DOI 10.1007/s00170-007-1154-1

ORIGINAL ARTICLE

The application of Taguchi's method in the experimental investigation of the laser sintering process

S. Dingal · T. R. Pradhan · J. K. Sarin Sundar · A. Roy Choudhury · S. K. Roy

Received: 21 December 2006 / Accepted: 29 June 2007 / Published online: 25 August 2007

Abstract The selective laser sintering (SLS) of iron powder has been investigated through a number of experiments statistically planned as per Taguchi L8 design. Seven input parameters, namely, laser peak power density, laser pulse on-time, laser scan speed, stepping distance (distance traveled between pulses), interval–spot ratio (ratio of laser scan line interval and laser spot diameter), size range of iron powder particles, and powder layer thickness, were selected for the investigation. Density, porosity, and hardness were considered for the characterization of the sintered samples. Analysis of the results show that these properties are significantly affected by these factors. A discussion on the probable physical phenomena contributing to such dependence and an attempt towards the optimization of the process have also been included.

Keywords Selective laser sintering · Rapid prototyping · Taguchi method · SLS · RP

S. Dingal · T. R. Pradhan · A. R. Choudhury (✉)
Department of Mechanical Engineering,
Indian Institute of Technology (IIT) Kharagpur,
Kharagpur 721302, India
e-mail: apuchoudhury@yahoo.com

J. K. S. Sundar
Center for Laser Processing of Materials,
International Advanced Research Centre for Powder Metallurgy and New Materials (ARCI),
Hyderabad 500005, India

S. K. Roy
Department of Metallurgical and Materials Engineering,
IIT Kharagpur,
Kharagpur 721302, India

1 Introduction

Selective laser sintering (SLS), with its capability for producing metallic and non-metallic shapes without part-specific tooling, is one of the main solid freeform fabrication (SFF) processes employed in rapid prototyping (RP). In this process, a part is built up layer by layer through the consolidation of powder particles with a focused laser beam that selectively scans the surface of the powder bed. Consolidation occurs either by actual fusion of the powder particles or by diffusion bonding.

Earlier, laser sintering had been utilized to build parts from polymeric materials like ABS (acrylonitrile butadiene styrene), nylon, glass-filled nylon, and polycarbonate plastics [1], while metallic materials like low-carbon steel, copper, titanium, superalloy, etc. have also been tried [2–4]. However, the actual production of metallic objects by SLS is much more complicated and has been pursued through two different approaches, known as indirect and direct laser sintering [5].

Indirect laser sintering is the less challenging approach of the two and involves the sintering of metal powders either mixed with some form of a binder or coated with a polymer. Hence, powder particles are consolidated by the melting and binding capacity of low-melting-point polymers, which are eventually burnt off. The part is subsequently infiltrated with a low-melting-point metal. Selective laser sintering of a mixture of two different metal powders like Cu-Ni, Fe-Co, and W-Mo has also been investigated [3]. In such cases, the low-melting-point metals fuse early and, thus, aid the bonding process.

In direct laser sintering, high-density objects are created by the sintering of metal powders without the aid of any binders [5–7]. Research in recent years has identified the potential of this process to build metallic components that

can act as functional prototypes. In fact, with the proper choice of input conditions, SLS can build parts with microstructure and mechanical properties equivalent to or closely resembling those of parts produced by conventional manufacturing.

2 Literature review

A number of investigations are reported in the literature on the SLS of metal powders. An extensive review has been carried out by Agarwala et al. [8] on the production of components by the direct SLS of metal powders. Bourell et al. [9] have reported an overview on the basic principles of laser sintering and the bonding mechanism between powder particles. Kumar [10] has also made a review of SLS, where the development and progress of the process has been documented. Pham et al. [11] focused on the application of the SLS process and explained the technological capabilities of the process. Niu and Chang [12] reported on the SLS of high-speed steel powders with a 25-W continuous wave CO_2 laser. They concluded that the consolidation mechanism during the process changes with the increase in laser power from solid phase sintering through liquid phase sintering to total melting/solidification. Kathuria's [13] investigation was directed upon the fabrication of metal matrix composite parts using CO_2/Nd-YAG lasers, where the major focus was on the evolved microstructures. Schueren and Kruth [14] performed experiments on the sintering of Fe–Cu powder mixture using a Nd-YAG laser and proposed a melting/densification mechanism. Song [15] has reported on the direct sintering of pre-alloyed bronze powders with single spot, line, and layer on the powder bed without the use of any polymer binder or preheating. It is concluded that laser beam power, scan speed, and hatching distance exert an influence on the part quality characteristics. Williams and Deckard [16] investigated the method of energy deliverance to the powder medium during SLS and its effect on different operating parameters, like laser power, hatching distance, scan speed, beam spot size, etc. O'Neill et al. [17] suggested that porosity, which is a major problem in parts produced by SLS, can be tackled by infiltration with a low-melting-point metal. Abe et al. [18] reported that laser-sintered die materials (nickel-base, pre-alloyed) do not exhibit balling-up phenomenon, but the presence of defects like deflection and cracking were evident in the sintered mass. It was further suggested that a dual-laser scanning system could possibly reduce these defects. Murali et al. [19] reported on the mechanical and physical properties of laser-sintered iron–graphite powder mixture and emphasized the potential of the process in developing self-lubricating porous bearing materials. According to Simchi and Pohl [20], the densification behavior and the evolved microstructural features of iron powders processed by direct laser sintering depend primarily upon specific energy input, scan rate, and scan distance. It has been proposed that the sintering process occurs by melting and solidification. Simchi et al. [21] have developed an iron-based powder blend for rapid tooling using a direct laser sintering process. The powder mixture consisted of different elements, such as Fe, C, Cu, Mo, and Ni. High sintering activities were obtained by tailoring the powder characteristics and optimizing the percentage of chemical constituents. The residual porosity was less than 5%.

Chatterjee et al. [22] carried out statistically designed experiments on the laser sintering of iron powder to investigate the effect of layer thickness and hatching distance on the sintered quality. Their study included an interesting discussion on the porosity of laser-sintered samples.

Dingal et al. [23] applied Taguchi's method (L8 design) to the SLS of iron powder to investigate the S/N ratio of the density and porosity of the sintered samples. It was found that the layer thickness had the most significant influence on the S/N ratio of the response parameters.

Miller et al. [24] carried out factorial experiments to express the strength of sintered samples as a function of laser power, scan speed, and spacing (hatching distance), and their respective interaction terms. The developed model took into account the variation of small and large beam spot sizes and the effect of heat loss on the strength of sintered samples. Hardro et al. [25] determined the optimal process parameters for the SLS of an elastomeric polymer using an experimental design approach. Laser power, laser scan spacing, and part bed temperature were the factors under consideration, while the dimensional accuracy and material strength of the sintered samples were the response characteristics. It was concluded that all of the factors, as well as their interactions, are statistically significant. Yang et al. [26] studied the shrinkage rate of laser-sintered parts through an experimental investigation using Taguchi's method. By the optimum choice of the factors, the shrinkage rate was reduced to insignificant levels. Reddy et al. [27] carried out an experimental work on SLS based on Taguchi's method (L8 design), where the influence of input factors (laser power, scan spacing, and part orientation, and their interactions) on part quality (surface roughness) was studied. Dongdong and Shen [28] studied the liquid phase sintering of a multi-phase Cu-based metal powder, where particle shape, size, and distribution were found to have significant influence on the sintered density and microstructural homogeneity. Kruth et al. [29] and Kruth and Kumar [30] carried out statistically designed experiments as per Taguchi L9 design to optimize the effect of scan spacing, layer thickness, and scan speed on the

hardness, surface roughness, and density of the sintered material. Bronze infiltration was performed to increase the density of the sintered samples. In another work, Kumar and Kruth [31] further investigated the infiltration of bronze into laser-sintered iron products and found it to be significantly improving the quality of porous sintered products in comparison to that of laser-melted products. Wang et al. [32] reported the direct SLS of WC–Co powder mixture in which an excellent simulation of energy absorption of laser radiation into powder material has been provided. It is shown that the highest energy absorption takes place slightly below the surface of the pre-placed powder. This shift in the point of maximum absorption from the surface to inside the powder layer was previously shown by Childs et al. [33]. Dongdong and Shen [34] carried out laser sintering with WC–Co as the reinforcement in a Cu–metal matrix, where the reduction of a proportion of WC–Co resulted in insufficient reinforcement, while its increase caused the agglomeration of WC particulates. Maeda and Childs [35] also worked on the possibility of forming a hard coating of WC–Co with bronze infiltration and presented sand abrasion test results on the obtained coatings. Kolosov et al. [36] proposed a procedure to estimate the powder layer quality in SLS by a heterogeneity coefficient. In the investigation, the hatch distance was found to have a profound influence on sintering precision and inner sintering quality. Simchi [37] established a simple sintering model in which the densification of metal powders was related to the laser specific energy input. The relation was dependent on the powder particle size, chemical composition, and oxygen content of the powders. Zhu et al. [38] reported that, in direct-laser-sintered metallic parts, the apparent density of the powder had the maximum influence on the final density of the sintered mass. Kruth et al. [39] applied selective laser melting (SLM) to a mixture of different metallic particles in an attempt to obtain high densification with good mechanical properties. Parameter adjustment and special scanning strategies were employed for optimization.

SLS has also been employed for customized scaffold development and tissue engineering [40–47] for the replacement and repair of damaged tissue, porous polymeric drug delivery systems [48–50], etc.

Earlier, researchers have investigated the process of laser sintering, where several input factors have been identified and studied by different groups. In the present work, seven input factors have been taken into consideration.

3 Objectives of the present work

The primary aim of the present investigation was to study the SLS of pure iron powder through statistically designed experiments following Taguchi L8 design in order to determine the significance of the process parameters affecting the quality of the sintered mass with respect to density, porosity, and hardness.

If the properties of parts developed by SLS are comparable to those of parts produced by conventional processing, single-piece and small-lot parts of complex geometry can be made by SLS, thus, circumventing the use of expensive part-specific tooling. In this respect, the present investigation reviews the reported work (Sect. 2) already done in this direction and attempts to statistically identify the important SLS parameters and their respective values that would permit the highly accurate and repeatable control over the properties of SLS products.

4 Design of experiments

4.1 Selection of parameters

It was envisaged to investigate the influence of the various laser process parameters through an L8 orthogonal array as suggested by Taguchi, where the inputs could be tested at two levels. It was further assumed that there exists no interaction between the factors considered in the experiments. The laser input parameters for the SLS process were:

(a) Peak power density [=pulse energy/(spot area*pulse on-time)], W, Watt/mm^2
(b) Particle size, P_s, μm
(c) Interval–spot ratio (=scan line interval/laser spot diameter), I, dimensionless
(d) Layer thickness, L, μm
(e) Stepping distance, S, μm
(f) Pulse on-time, T_{on}, ms
(g) Scan speed, S_s, mm/s

It should be mentioned here that the laser spot was kept constant. Some of the parameters involved in the SLS process are schematically presented in Fig. 1.

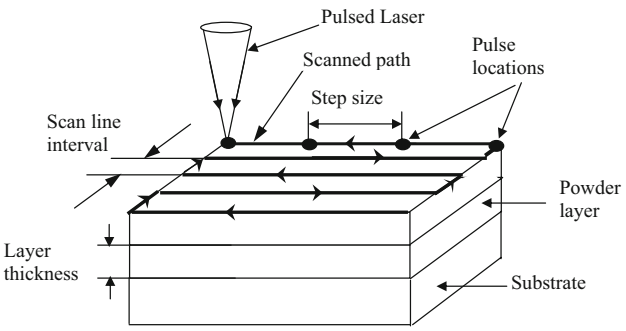

Fig. 1 Schematic diagram of the laser sintering process showing the relevant nomenclature

Table 1 L8 orthogonal array showing the choice of factors, their respective levels, and the corresponding response parametric values

Exp. no.	Input factors							Response parameters			
	W	P_s	I	L	S	T_{on}	S_s	P	ρ	H	H_{cm}
1	1,500	46–65	0.25	200	250	5	2.5	2.57	7.68	244.3	205.1
2	1,500	46–65	0.25	400	450	10	5	7.96	7.30	236.4	180.1
3	1,500	106–125	0.40	200	250	10	5	2.19	7.71	294.5	175.1
4	1,500	106–125	0.40	400	450	5	2.5	5	7.52	318.8	185.2
5	3,000	46–65	0.40	200	450	5	5	2.6	7.63	406.8	207.9
6	3,000	46–65	0.40	400	250	10	2.5	5.11	7.31	290.4	173.5
7	3,000	106–125	0.25	200	450	10	2.5	2.06	7.72	292.8	168.3
8	3,000	106–125	0.25	400	250	5	5	2.42	7.69	288.1	174.2

4.2 Statistical design

There are several ways to statistically design an experimental investigation, but the most frequently used and exhaustive approach is a full factorial experiment. However, for full factorial experiments, there are 2^k possible combinations that must be tested (where k is the number of factors, each at two levels). Therefore, it becomes increasingly difficult to carry out investigations when the number of factors becomes significantly high. In order to minimize the number of tests required, fractional factorial experiments (FFEs) were developed [51]. FFEs allow only a portion of the total possible combinations to estimate the main effects of factors and some of their interactions. Taguchi [52] developed a family of FFE matrices which eventually reduce the number of experiments, but still provide sufficient information. The conclusions can also be associated with statistical levels of confidence. In Taguchi's methodology, the factors affecting the process quality can be divided into two types: control and noise factors [52–54]. Control factors are those set by the experimenter and are easily adjustable. These factors are expected to have a significant influence over the quality of the product. Noise factors, on the other hand, are those undesired variables that are difficult, impossible, or expensive to control, such as the ambient temperature, humidity, and the aging of parts.

The major steps in the application of Taguchi's method in an experimental investigation are: (1) to identify the factors/interactions; (2) to identify the number of levels of each factor; (3) to determine the values of the level of the factors; (4) to select an appropriate orthogonal array (OA); (5) to assign the factors/interactions to columns of the OA, (6) to conduct the experiments, (7) to analyze the data and determine the optimal levels; and (8) to conduct the confirmation experiments.

Two-level factors are recommended by Taguchi [52] for an initial experiment. If the factors and their interactions are not more than 7, a possible matrix is an eight-trial orthogonal array, which is labeled as an L8 matrix. The actual levels of the factors selected in this investigation for the L8 design are shown in Table 1 (with responses included in latter columns). The Taguchi L8 design is a statistical plan for conducting eight experiments with a maximum of seven input factors (or input factors and their interactions, seven in all) set at two levels and arranged in

Table 2 Percentage composition of the impurities present in the iron powder (in wt%)

Trade name of powder	C	O	S	Mn	P	Si	Fe
Atomet 86 (QMP Powders, Canada)	0.04	0.5	0.005	Trace	Trace	Trace	Rest

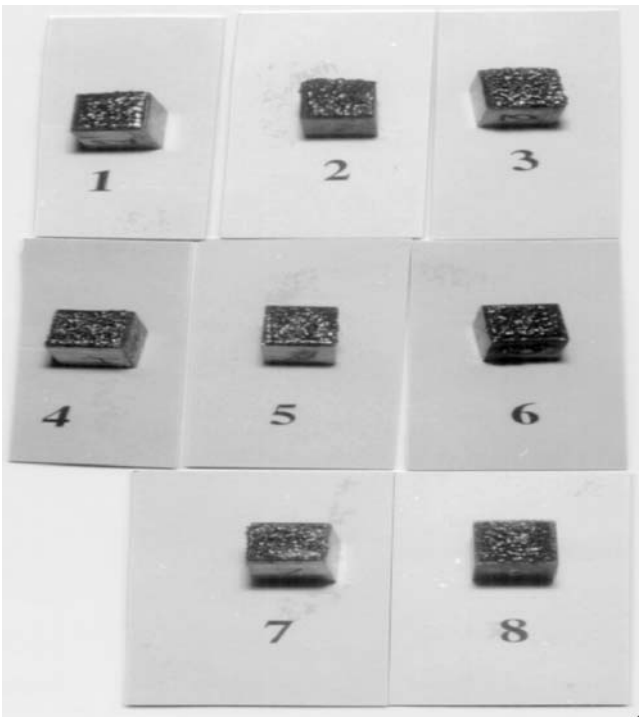

Fig. 2 Laser-sintered samples named as per experiment no. in the L8 design in Table 1

Table 3 Replications and signal-to-noise (S/N) values for response parameters

Exp. no.	Porosity, %			Density, gm/cc			Top surface microhardness, HV			Cross microhardness, HV		
	Replications		S/N db	Replications		S/N db	Replications		S/N db	Replications		S/N db
	P_1	P_2		ρ_1	ρ_2		H_1	H_2		H_{c1}	H_{c2}	
1	2.53	2.61	24.94	7.71	7.65	27.44	240.6	248	−14.3	205	205.2	16.9
2	8.12	7.80	12.90	7.32	7.28	30.96	238.2	234.6	−8.11	180	180.2	16.9
3	2.2	2.18	36.98	7.69	7.73	30.96	292.2	296.9	−10.4	175	175.3	13.4
4	5.00	5.00	36.98	7.54	7.50	30.96	320.1	317.5	−5.28	185	185.4	10.9
5	2.58	2.62	30.96	7.68	7.58	23.01	404.8	408.8	−9.03	208	207.9	23.0
6	5.08	5.14	27.44	7.29	7.33	30.96	293.4	287.4	−12.5	173	173.3	13.4
7	2.09	2.03	27.44	7.76	7.68	24.94	291.7	293.9	−3.83	168	168.7	6.10
8	2.52	2.32	16.98	7.73	7.67	27.44	284.5	291.7	−14.1	174	174.5	9.03

orthogonal arrays. It is actually a 1/16 FFE for seven input factors. In this method, each factor is assigned a column and each row represents an experiment with a unique combination of factor levels. The maintenance of orthogonality between columns ensures that, for every factor, four tests would be carried out at one level, while the remaining four would be performed at the other level. This permits the simultaneous evaluation of the effects of several factors with the minimum number of experiments. The disadvantage is that there is considerable "confounding" or overlapping of factor and interaction influences due to the drastic reduction in the number of experiments from a full factorial design of 128 experiments.

In data analysis, signal-to-noise (S/N) ratios are utilized to achieve control over the response, as well as to reduce the variability of the response. Finally, analysis of variance (ANOVA) has been used to calculate the statistical confidence associated with the conclusions drawn.

5 Experiments

5.1 Description of experimental setup

The laser system employed for the experiments was a JK 704 GSI Lumonics pulsed-mode Nd-YAG laser capable of delivering 400 Watts average power in pulsed-mode operation, where the radiation had a wavelength of 1.064 μm in the near-infrared range. A four-axis computerized numerical control (CNC) system was used for job manipulation. A PC was interfaced with the CNC controller to guide the movement of table in both X and Y directions. A charged couple display (CCD) viewing unit was coupled to the system to precisely align and view the position and movement of the job during processing.

5.2 Materials

Iron powder was employed for the sintering experiments with a chemical composition as presented in Table 2. Two different particle size ranges of this iron powder, 46–65 μm and 106–125 μm, were selected for the sintering experiments. Prior to laser processing, the powders were heated to 600°C in H_2 atmosphere to ensure that there were no oxides on the powders.

5.3 Experimental procedure

The SLS experiments were conducted inside an inert gas chamber to avoid any oxidation during the sintering operation. A powder layer (the first layer) of required thickness was applied over a mild steel substrate of 10×10-mm cross-section. After this, the desired laser operating parameters were fed to the laser's control panel, while the programmed motion sequence was fed into the computer for guiding the track

Table 4 Analysis of variance (ANOVA) for the average values of response parameters

Porosity, %				Density, gm/cc				Top surface microhardness, HV				Mean cross hardness, HV			
SF	SS	df	F	SF	SS	df	F	SF	SS	df	F	SF	SS	df	F
W	3.82	1	310[a]	P_s	0.064	1	7.26[b]	I	7,743	1	6.5[b]	P_s	508.8	1	18.6[b]
P_s	5.39	1	438[a]	L	0.105	1	11.8[b]					L	235.4	1	8.61[b]
L	15.3	1	1,244[a]									T_{on}	710.6	1	26[a]
S	3.55	1	288[a]												
T_{on}	2.79	1	227[a]												
E	0.02	2		E	0.044	5		E	7,145	6		E	109.3	4	

[a] 99% confidence, [b] 95% confidence, [c] 90% confidence

SF=significant factor, SS=sum of squares of each factor, df=degree of freedom, F=*f*-test value, E=pooled-up errors

Table 5 ANOVA for the S/N values of response parameters

Porosity, %				Density, gm/cc				Top surface microhardness, HV				Mean cross hardness, HV			
SF	SS	df	F	SF	SS	df	F	SF	SS	df	F	SF	SS	df	F
P_s	61.29	1	13.31[b]	W	24.42	1	6.01[c]	S	79.51	1	17.37[a]	P_s	119.2	1	9.39[b]
I	313.7	1	68.15[a]	L	24.42	1	6.01[c]								
L	84.63	1	18.38[b]												
S_s	45.01	1	9.777[c]												
E	13.81	3		E	20.29	5		E	27.46	6		E	76.09	6	

[a] 99% confidence, [b] 95% confidence, [c] 90% confidence
SF=significant factor, SS=sum of squares of each factor, df=degree of freedom, F=*f*-test value, E=pooled-up errors

movement. The inert gas (Argon) flow rate was maintained at 5 lpm. Subsequently, sintering of the first applied layer was carried out by to-and-fro passes of the scanning laser beam over the powder surface (Fig. 1). After the sintering of the first layer, the whole procedure was repeated several times until a sintered mass height of 2 mm was achieved.

The density measurement of each sintered mass was performed following Archimedes principle. In such an exercise, the weights were measured with the help of an electronic balance (SARTORIUS Gmbh) with an accuracy ±0.01 mg. The porosity contained in each sintered mass was measured with the aid of a DMLM image analyzer. The polished specimen surface was examined under the Leica Microscope attached to the DMLM image analyzer. A series of photographs were captured and the point-counting method was adopted for determining the volume fraction of porosity. In the point-counting method, a 10×10 grid was placed on the microstructure and the number of points falling on the pores was counted. Experiments were repeated on 100 locations to estimate the average volume fraction of the pores.

The top surfaces of the samples were lightly ground to obtain a flat surface, which would facilitate hardness measurement. Microhardness ($HV_{0.5}$) on the top surface (after grinding) and cross-section (at a point 500 microns below the ground top surface) was measured on a microhardness testing machine (Leco M-400-H1) with a 500-g load. The microstructural features of the sintered samples were examined under the JOEL SEM (scanning electron microscope), model JSM 5800.

6 Results and discussions

6.1 Experimental results and statistical analysis

Initially, a number of experiments were conducted to determine the domain of input parameters where the occurrence of balling phenomenon is not very pronounced. These experiments successfully allowed the investigators to select the levels of factors such that balling was ultimately not a major contributing physical phenomenon. It was found that, in general, at higher peak power density values, the balling phenomenon was less pronounced.

The laser-sintered samples are shown in Fig. 2, where the samples are numbered as per the experiment no. in the Taguchi L8 design in Table 1.

The porosity, density, top surface and cross-sectional microhardness values of the samples were measured (as discussed in Sect. 5.3 and as shown in Table 1) and statistical analysis was carried out to determine the S/N ratios (Table 3) and *F*-test values (Tables 4 and 5) obtained by implementing the pooling up of errors.

S/N ratios were calculated as S/N=−10*log S_e, where S_e is the standard deviation within a trial. This makes the S/N ratios completely independent of the average values of the responses and dependent only on variation [52]. Average values of the (a) responses and that of their respective (S/N) values for significant factor levels are shown in Tables 6, 8, 10, 12 and Tables 7, 9, 11, 13, respectively.

It is observed that the layer thickness L, particle size range of the powder material P_s, laser peak power density W, pulse stepping distance S, and the pulse on-time T_{on} have significant influence over the occurrence of porosity in the laser-sintered samples (Table 6). Among these, the effect of variation in layer thickness on porosity is the most pronounced. Higher layer thickness, lower laser peak power density, lower powder particle size range, higher stepping distance, and higher laser pulse on-time tend to produce higher porosity in the sintered masses and vice versa (Table 7).

The ANOVA for the S/N ratios of porosity values (Table 5) reveals that the particle size range P_s of the powder, interval–spot ratio I, layer thickness L, and laser scanning speed S_s are significant in influencing the variation in porosity values.

Table 6 Average porosity for significant factor levels

W	Average porosity	P_s	Average porosity	L	Average porosity	S	Average porosity	T_{on}	Average porosity
1,500	4.43	46–65	4.56	200	2.355	250	3.0725	5	3.1475
3,000	3.0475	106–125	2.917	400	5.1225	400	4.405	10	4.33

Table 7 Average S/N ratios of porosity for significant factor levels

P_s	Average (S/N) of porosity	I	Average (S/N) of porosity	L	Average (S/N) of porosity	S_s	Average (S/N) of porosity
46–65	24.06	0.25	20.565	200	30.08	2.5	26.585
106–125	29.595	0.4	33.09	400	23.575	5	27.07

Table 7 shows that higher levels of powder layer thickness and lower levels of particle size range, interval–spot ratio, layer thickness, and laser scanning speed are significant in reducing the variation in porosity values.

Powder layer thickness L and particle size range P_s were found to have significant influence on the density of the sintered samples (Table 4). The occurrence of lower density was observed in the case of higher layer thickness and lower particle size range (Table 8). Once again, the effect of layer thickness on density was the most pronounced.

The ANOVA (S/N ratios) of density values (Tables 5 and 9) reveals that higher levels of W and lower levels of L are significant in reducing variation in density values.

The interval–spot ratio I has a significant effect on the top surface microhardness of the sintered mass (Table 4). Lower levels of I tended to reduce the variation in the value of top surface microhardness (Table 10).

The stepping distance S has a significant effect on the variation of top surface microhardness (Table 5) and lower values of S tended to reduce its variation (Table 11).

The powder particle size range P_s, powder layer thickness L, and laser pulse on-time T_{on} had a significant influence on the cross-sectional microhardness of the sintered mass (Table 4) and lower levels of these factors tended to increase its value (Table 12).

Lower values of the powder particle size range P_s tended to reduce the variation of cross-sectional microhardness of the sintered mass (Tables 5 and 13).

Table 14 lists the significant factors for the responses and their respective variations.

7 Discussion

When layer thickness is high, there is a chance that the powder in the layer would be insufficiently heated and complete melting would not occur. This increases the probability of the occurrence of pores inside the sintered material. Similarly, lower levels of laser peak power density would be insufficient to completely melt the metal powder and, hence, can result in higher porosity. These are supported by the observations made from the statistical calculations in the previous section.

From the statistical calculations, it is observed that a higher particulate size range gives rise to a lower value of porosity and vice versa. This is not very obvious and, hence, it would be interesting to discuss this point in detail. If the powder is coarse-grained, inter-particular gaps are larger and a substantial fraction of the laser light can reach through these gaps to an appreciable depth inside the powder layer [32, 33]. Thus, heat generation (as a result of energy absorption) for a higher particulate size range would take place uniformly throughout the layer, leading to uniform and instantaneous melting, together with low radiation and convection losses. Hence, inside the layer, the major part of the heating could be through the direct absorption of laser energy.

On the contrary, if the powder is fine-grained, the relatively smaller inter-particular gaps prevent a major part of the laser light from reaching into the depth of the powder layer such that the laser heating is mainly concentrated at the surface. Hence, inside the layer, the major part of the heating could be through the conduction of heat energy from the surface of the powder layer. This conduction takes time (compared to direct laser energy absorption) and is directional, leading to slow non-uniform melting, higher radiative and convective losses. This phenomenon has a high probability of producing insufficient melting, which is one of the major reasons for pore or void formation. Hence, fine-grained powders could possibly give rise to higher porosity and vice versa.

A high level of laser pulse on-time is observed to produce higher porosity. This phenomenon is also not very obvious, as longer exposure to laser radiation should lead to less chances of insufficient melting. However, longer periods of heat addition could also result in the overheating

Table 8 Average density for significant factor levels

P_s	Average density	L	Average density
46–65	7.48	200	7.685
106–125	7.66	400	7.455

Table 9 Average S/N ratios of density for significant factor levels

W	Average (S/N) of density	L	Average (S/N) of density
1,500	30.08	200	26.5875
3,000	26.5875	400	30.08

Table 10 Average top surface microhardness for significant factor levels

I	Average top surface microhardness
0.25	265.4
0.4	327.625

Table 11 Average S/N ratio of top surface microhardness for significant factor levels

S	Average S/N of top surface microhardness
250	−12.825
450	−6.5625

Table 13 Average S/N ratio of cross-sectional microhardness for significant factor levels

P_s	Average S/N of cross microhardness
46–65	13.1825
106–125	14.225

and boiling of the melt, which can lead to vapor entrapment and, thus, result in higher porosity.

Experimental results (Table 4) show that layer thickness and particle size are factors that affect both density and porosity, and have the most significant influences on the two responses. Higher particle size and lower layer thickness yield lower porosity and higher density. From this observation, it can be inferred that the same physical feature is affecting density and porosity and, in the present case, it may be identified as the closed pores inside the sintered matrix.

The density of the sintered samples has been measured by Archimedes' principle, while porosity has been measured by image processing. Hence, while density measurement is affected only by closed pores, the porosity measurement yields the total porosity. In spite of this fact, there is considerable correlation between the density and porosity values. This suggests that closed pores are predominating over open, interconnected pores in the sintered matrix.

Top surface microhardness has been found to be affected only by the interval–spot ratio. It is found that, laser spot size remaining same, if the interval–spot ratio is reduced (so that the interval between successive laser paths decrease), the hardness of the sintered mass decreases. This is because the lower value of path interval results in the annealing of previously sintered material, which has a softening effect.

It is found that lower levels of powder particle size range P_s, layer thickness L, and laser pulse on-time T_{on} result in higher values of hardness. This is expected in the case of lower laser pulse on-time, as higher cooling rates are produced. It is also expected in the case of lower layer thickness, where the solid substrate (having higher thermal conductivity than the powder metal) is closer to the heated powder surface. This results in a higher cooling rate. In the case of fine powder particles, bulk heating is slower than that in coarse powder (as discussed in the beginning of this section), but the cooling rate would be higher in finer powders in comparison to that in coarse powders, as the surface temperature is very high due to the concentration of heat energy at the surface.

Table 12 Average cross-sectional microhardness for significant factor levels

P_s	Average cross hardness	L	Average cross hardness	T_{on}	Average cross hardness
46–65	191.65	200	189.1	5	193.1
106–125	175.7	400	178.25	10	174.25

7.1 Metallurgical observations

The laser-sintered samples were metallographically polished and their surfaces were observed under an optical microscope as well as SEM in unetched and etched conditions. A typical SEM micrograph of the top surface of the sintered mass, as depicted in Fig. 3, clearly reveals that it is practically free from the occurrence of balling phenomenon, which was observed in earlier investigations [8, 15, 19]. Further, the microstructure reveals distinct differences between substrate and sintered layers (Fig. 4). It also shows the densification of the sintered layers into a consolidated mass. Figure 5 shows a round pore in the sintered metal matrix, which is evident of evolved gases from the sintered matrix/engulfed air bubble. It is possibly due to the evolution of gases during the solidification process. Figure 6, however, shows a triangular pore, which is more common in conventional sintering, where grain growth from a number of nucleation points become arrested together to form a triangular pore [55, 56]. This shows that, even in laser sintering, the mechanism of conventional sintering is active. This is probably due to the fact that conventional sintering occurs during subsequent passes of the laser.

Table 14 Factors affecting the average values and variation of porosity, density, top hardness, and cross hardness

Factors	Porosity		Density		Top hardness		Cross hardness	
	Raw data	Variation	Raw data	Variation	Raw data	Variation	Raw data	Variation
W	√			√				
P_s	√	√	√				√	√
I		√			√			
L	√	√	√	√			√	
S	√					√		
T_{on}	√						√	
S_s		√						

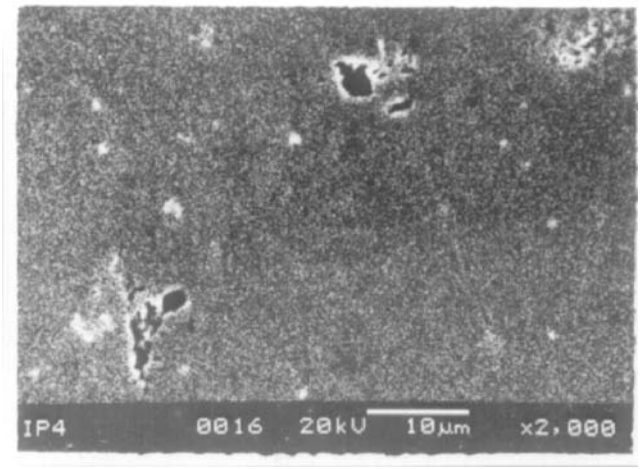

Fig. 3 Top surface of a laser-sintered sample

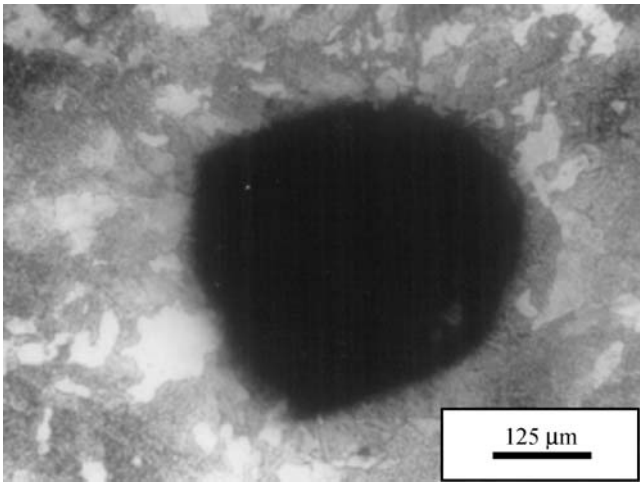

Fig. 5 A round pore in a sintered metal matrix

The trail of laser track, as evidenced in Fig. 4, suggests that melting of the powders occurred during the laser–powder interaction and, finally, a consolidated mass was formed.

7.2 Optimization

According to Taguchi [52], the optimization of a system can be achieved by: (a) robustness: setting the levels of parameters in such a way that variation in the output is minimized; (b) setting the levels of the rest of the parameters such that the desired levels of the output parameters are reached.

In the present investigation, it is desirable to have low porosity, high density, high top and cross-sectional microhardness.

Following this procedure, the following observations can be made:

(a) A higher level of laser peak power density W (=3,000 Watts/mm^2) is chosen, as it reduces porosity and reduces the variation in density.

(b) The particle size range P_s is set to its lower level of 46–65 microns, as it decreases the variation in porosity, increases cross-sectional hardness, and decreases its variation. However, a lower level of P_s would increase porosity and decrease density to some extent.

(c) A lower level of stepping distance S (250 microns) is selected, as it reduces porosity and reduces variation in top surface microhardness.

(d) The scanning speed S_s is set to its lower level of 2.5 mm/s, where it reduces the variation in porosity.

(e) The interval–spot ratio I is set to its higher level of 0.4, where it significantly increases top surface microhardness. However, it would increase the variation in porosity, but this cannot be avoided.

(f) The layer thickness L is set to the lower level of 200 microns, as it decreases porosity, increases density, reduces variation in density, and increases cross-sectional hardness. However, it would also increase the variation in porosity to some extent.

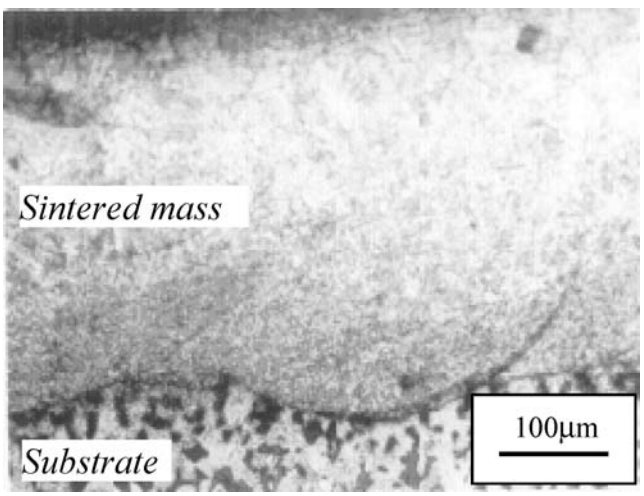

Fig. 4 Densified sintered layers and substrate

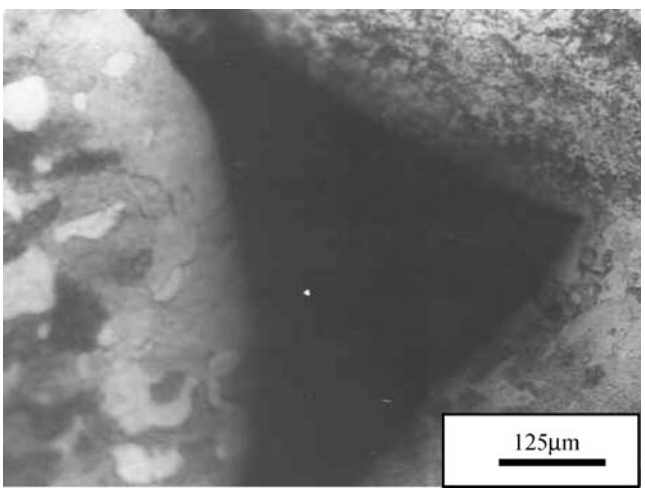

Fig. 6 A triangular pore in a sintered matrix

(g) The laser pulse on-time T_{on} is set to its lower value of 5 ms, as it reduces porosity and increases cross-sectional hardness.

8 Conclusions

(a) The balling phenomenon can be substantially reduced during laser sintering and, in the present investigation, the laser peak power density had the greatest influence on the phenomenon.
(b) The sintering process in the present work has been found to occur by melting and solidification.
(c) There are various forms of influence of the seven factors selected for the investigation of the four responses and their respective variations in selective laser sintering, and they have been duly identified and explained.
(d) Density and porosity show a high level of correlation that indicates that most of the pores are closed in nature.
(e) Conventional sintering mechanisms are active in laser sintering as well.

Acknowledgement The authors are thankful to the Department of Science and Technology, Government of India, for the financial support towards this project work. They are also thankful to Dr. S. V. Joshi, Director, CLPM Laboratory, ARCI, Hyderabad, India, for kindly extending the facilities for conducting experiments on laser sintering and for providing useful advice and suggestions.

References

1. Ho HCH, Cheung WL, Gibson I (2002) Effects of graphite powder on the laser sintering behaviour of polycarbonate. Rapid Prototyping Journal 8:233–242
2. Zhu HH, Lu L, Fuh JYH (2003) Development and characterisation of direct laser sintering Cu-based metal powder. J Mater Process Technol 140:314–317
3. Steen WM (1998) Laser material processing, 2nd edn. Springer, London, UK
4. Das S, Fuesting TP, Danyo G, Brown LE, Beaman JJ, Bourell DL (2000) Direct laser fabrication of superalloy cermet abrasive turbine blade tips. Mater Des 21:63–73
5. Kathuria YP (1999) Microstructuring by selective laser sintering of metallic powder. Surf Coat Technol 116–119:643–647
6. Tolochko NK, Laoui T, Khlopkov Y, Mozzharov S, Titov V, Ignatiev M (2000) Absorptance of powder materials suitable for laser sintering. Rapid Prototyping J 6:155–161
7. Duley WW (1986) Laser surface treatment of metals. NATO-ASI Series (E) 115:3–15
8. Agarwala M, Bourell D, Beaman J, Marcus H, Barlow J (1995) Direct selective laser sintering of metals. Rapid Prototyping J 1:26–36
9. Bourell DL, Marcus HL, Barlow JW, Beaman JJ (1992) Selective laser sintering of metals and ceramics. Int J Powder Metall 28:369–381
10. Kumar S (2003) Selective laser sintering: a qualitative and objective approach. JOM 55:43–47
11. Pham DT, Dimov SS, Lacan F (2000) The RapidTool process: technical capabilities and applications. Proc Inst Mech Eng B 214:107–116
12. Niu HJ, Chang ITH (1999) Selective laser sintering of gas and water atomized high speed steel powders. Scripta Mater 41:25–30
13. Kathuria YP (2000) Metal rapid prototyping via a laser generating/selective sintering process. Proc Inst Mech Eng B 214:1–9
14. Schueren BVD, Kruth J-P (1995) Powder deposition in selective metal powder sintering. Rapid Prototyping J 1:23–31
15. Song Y (1997) Experimental study of the basic process mechanism for direct selective laser sintering of low-melting metallic powder. Ann CIRP 46:127–130
16. Williams JD, Deckard CR (1998) Advances in modeling the effects of selected parameters on the SLS process. Rapid Prototyping J 4:90–100
17. O'Neill W, Sutcliffe C J, Morgan R, Landsborough A, Hon KKB (1999) Investigation on multi-layer direct metal laser sintering of 316 L stainless steel powder beds. Ann CIRP 48:151–154
18. Abe F, Osakada K, Shiomi M, Uematsu K, Matsumoto M (2001) The manufacturing of hard tools from metallic powders by selective laser melting. J Mater Process Technol 111:210–213
19. Murali K, Chatterjee AN, Saha P, Palai R, Kumar S, Roy SK, Mishra PK, Roy Choudhury A (2003) Direct selective laser sintering of iron-graphite powder mixture. J Mater Process Technol 136:179–185
20. Simchi A, Pohl H (2003) Effects of laser sintering processing parameters on the microstructure and densification of iron powder. Mater Sci Eng A 359:119–128
21. Simchi A, Petzoldt F, Pohl H (2003) On the development of direct metal laser sintering for rapid tooling. J Mater Process Technol 141:319–328
22. Chatterjee AN, Saha P, Kumar S, Mishra PK, Roy Choudhury A (2003) An experimental design approach to selective laser sintering of low carbon steel. J Mater Process Technol 136:151–157
23. Dingal S, Pradhan TR, Sundar S, Roy Choudhury A, Roy SK (2004) Experimental investigation of selective laser sintering of iron powder by application of Taguchi method. In: Proceedings of the 2004 Laser Assisted Net Shape Engineering conference (LANE 2004), Erlangen, Germany, September 2004, pp 445–456
24. Miller D, Deckard C, Williams J (1997) Variable beam size SLS workstation and enhanced SLS model. Rapid Prototyping J 3:4–11
25. Hardro PJ, Wang J-H, Stucker BE (1999) Determining the parameter settings and capability of a rapid prototyping process. Int J Ind Eng—Theory 6:203–213
26. Yang H-J, Hwang P-J, Lee S-H (2002) A study on shrinkage compensation of the SLS process by using the Taguchi method. Int J Mach Tool Manu 42:1203–1212
27. Reddy TAJ, Kumar YR, Rao CSP (2006) Determination of optimum process parameters using Taguchi's approach to improve the quality of SLS parts. In: Proceedings of the 17th IASTED International Conference on Modelling and Simulation (MS 2006), Montreal, Quebec, Canada, May 2006, pp 228–233
28. Dongdong G, Shen Y (2007) Effects of dispersion technique and component ratio on densification and microstructure of multi-component Cu-based metal powder in direct laser sintering. J Mater Process Technol 182:564–573
29. Kruth J-P, Froyen L, Kumar S, Rombouts M, Van Vaerenbergh J (2004) Study of laser-sinterability of iron-based powder mixture. In: Proceedings of the 10th European Forum on Rapid Prototyping, Paris, France, September 2004, pp S3–S8
30. Kruth J-P, Kumar S (2005) Statistical analysis of experimental parameters in selective laser sintering. Adv Eng Mater 7:750–755
31. Kumar S, Kruth J-P (2007) Effect of bronze infiltration into laser sintered metallic parts. Mater Design 28:400–407
32. Wang XC, Laoui T, Bonse J, Kruth J-P, Lauwers B, Froyen L (2002) Direct selective laser sintering of hard metal powders:

experimental study and simulation. Int J Adv Manuf Technol 19:351–357
33. Childs THC, Hauser C, Taylor CM, Tontowi AE (2000) Simulation and experimental verification of crystalline polymer and direct metal selective laser sintering. In: Proceedings of the 11th Annual Solid Freeform Fabrication Symposium, Austin, Texas, August 2000, pp 100–109
34. Dongdong G, Shen Y (2006) WC–Co particulate reinforcing Cu matrix composites produced by direct laser sintering. Mater Lett 60:3664–3668
35. Maeda K, Childs THC (2004) Laser sintering (SLS) of hard metal powders for abrasion resistant coatings. J Mater Process Technol 149:609–615
36. Kolosov S, Vansteenkiste G, Boudeau N, Gelin JC, Boillat E (2006) Homogeneity aspects in selective laser sintering (SLS). J Mater Process Technol 177:348–351
37. Simchi A (2006) Direct laser sintering of metal powders: mechanism, kinetics and microstructural features. Mater Sci Eng A 428:148–158
38. Zhu HH, Fuh JYH, Lu L (2007) The influence of powder apparent density on the density in direct laser-sintered metallic parts. Int J Mach Tool Manu 47:294–298
39. Kruth J-P, Froyen L, Van Vaerenbergh J, Mercelis P, Rombouts M, Lauwers B (2004) Selective laser melting of iron-based powder. J Mater Process Technol 149:616–622
40. Tan KH, Chua CK, Leong KF, Cheah CM, Cheang P, Abu Bakar MS, Cha SW (2003) Scaffold development using selective laser sintering of polyetheretherketone–hydroxyapatite biocomposite blends. Biomaterials 24:3115–3123
41. Chua CK, Leong KF, Tan KH, Wiria FE, Cheah CM (2004) Development of tissue scaffolds using selective laser sintering of polyvinyl alcohol/hydroxyapatite biocomposite for craniofacial and joint defects. J Mater Sci—Mater Med 15:1113–1121
42. Tan KH, Chua CK, Leong KF, Naing MW, Cheah CM (2005) Fabrication and characterisation of 3D polyetherketone/hydroxyapatite biocomposite scaffolds using laser sintering Proc Inst Mech Eng H 219:183–194
43. Naing MW, Chua CK, Leong KF, Wang Y (2005) Fabrication of customized scaffolds using computer aided design and rapid prototyping techniques. Rapid Prototyping J 11:249–259
44. Wiria FE, Leong KF, Chua CK, Liu Y (2007) Poly-ε-caprolatone/hydroxyapatite for tissue engineering scaffold fabrication using selective laser sintering. Acta Biomater 3:1–12
45. Wiria FE, Chua CK, Leong KF, Quah ZY, Chandrasekaran M, Lee MW (2007) Improved biocomposite development of poly(vinyl alcohol) and hydroxyapatite for tissue engineering scaffolds fabrication using selective laser sintering. J Mater Sci—Mater Med (in press)
46. Simpson RL, Wiria FE, Amis AA, Chua CK, Leong KF, Hansen UN, Chandrasekaran M, Lee MW (2007) Development of a 95/5 poly(L-lactide-co-glycolide)/hydroxylapatite and β-tricalcium phosphate scaffold as bone replacement material via selective laser sintering. J Biomed Mater Res B—Appl Biomater (in press)
47. Tan KH, Chua CK, Leong KF, Cheah CM, Gui WS, Tan WS, Wiria FE (2005) Selective laser sintering of biocompatible polymers for applications in issue engineering. Biomed Mater Eng 15:113–124
48. Leong KF, Chua CK, Gui WS, Verani (2006) Building porous biopolymeric microstructures for controlled drug delivery devices using selective laser sintering. Int J Adv Manuf Tech 31:483–489
49. Cheah CM, Leong KF, Chua CK, Low KH, Quek HS (2002) Characterization of microfeatures in selective laser sintered drug delivery devices. Proc Inst Mech Eng H 216(6):369–383
50. Leong KF, Wiria FE, Chua CK, Li SH (2007) Characterization of a poly-ε-caprolactone polymeric drug delivery device built by selective laser sintering. Biomed Mater Eng 17:147–157
51. Cochran WG, Cox GM (1992) Experimental designs, 2nd edn. Wiley, New York
52. Ross RJ (1989) Taguchi techniques for quality engineering. McGraw-Hill, New York
53. Ryan NE (1988) Taguchi methods and QFD: hows and whys for management. ASI Press, Dearborn, Michigan
54. Peace GS (1992) Taguchi methods: a hands-on approach. Addison-Wesley, Reading, Massachusetts
55. Lenel FV (1980) Powder metallurgy—principles and applications. Metal Powder Industries Federation, Princeton, New Jersey
56. Svoboda J, Riedel H (1995) Quasi-equilibrium sintering for coupled grain-boundary and surface diffusion. Acta Mater 43:499–506